MAS NMR study of the photoreceptor phytochrome

Rohmer, T.

Chapter 1

Introduction

1.1 Phytochrome

1.1.1 The phytochrome superfamily

The dominant factor regulating development and behavior of photosynthetic organisms is light, which provides both the energy necessary for growth and metabolism as well as the sensory information needed for adaptation to the environment. In order to sense light, plants use photoreceptors that perceive different areas of the electromagnetic spectrum [1–3]. Photoreceptors are proteins that bind a chromophore which undergoes a photochemical reaction upon absorption of light at a specific wavelength.

The phytochromes form a family of photoreceptors that is collectively defined by the use of a bilin chromophore (see section 1.1.3). Phytochrome pigments were first characterized in higher plants in the 1950's [4]. Vierstra and Quail [5] isolated the full-length phytochrome protein from *Avena sativa* in 1982 and the complete amino acid sequence of this phytochrome was obtained in 1985 [6]. More recently, polygenetic and biochemical studies have dramatically expanded the phytochrome superfamily to other domains of life. Phytochromes were discovered in proteobacteria, cyanobacteria, fungi and possibly slime moulds. Karniol *et al.* [7] organized the members of the phytochromes superfamily into distinct subfamilies that include plant phytochromes, bacteriophytochromes, cyanobacterial phytochromes, fungal phytochromes and a collection of phytochrome-like sequences (Fig. 1.1).

The phytochrome properties are triggered by the intrinsic photochemical

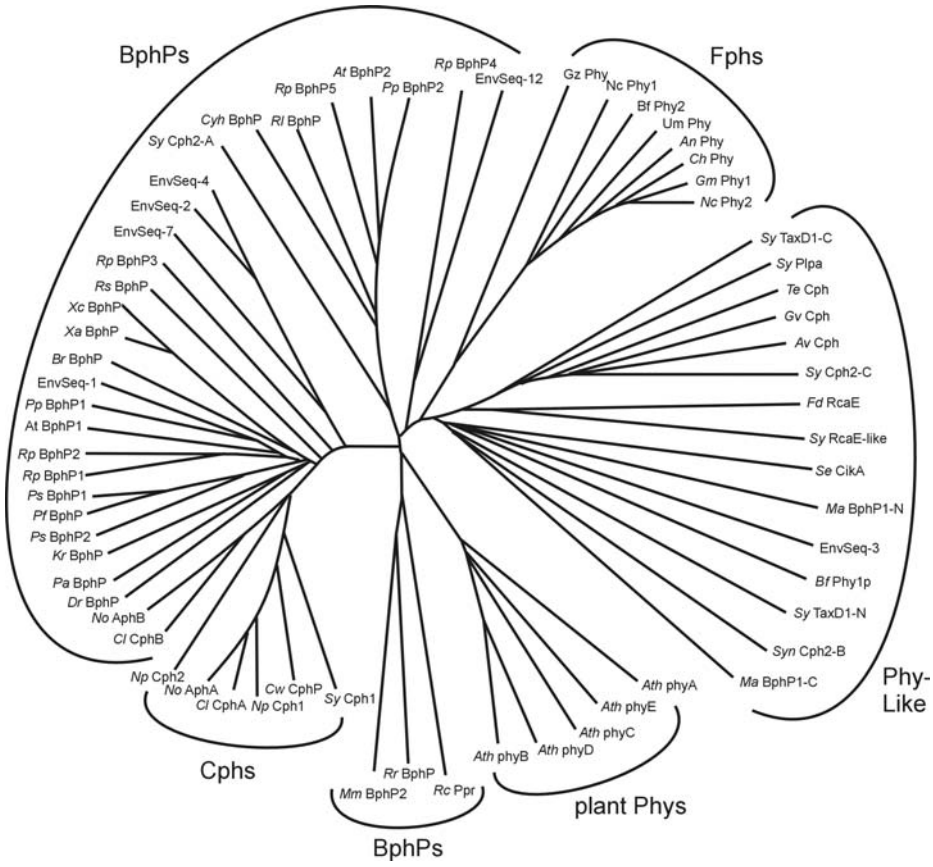

Figure 1.1: Phylogenetic tree of the phytochrome superfamily based on alignment of the GAF domain (adapted from [7]).

activity of their bilin (or linear open-chain tetrapyrrole) prosthetic group within the protein matrix (Fig. 1.2A). It allows phytochromes to occur in two photointerconvertible states, the red-light Pr ($\lambda_{max} \sim 660$ nm) and far-red-light Pfr ($\lambda_{max} \sim 710$ nm) absorbing states (Fig. 1.2B). The biological activity of phytochromes is related to the Pr/Pfr ratio, which is determined by the light environment. The plant Phys, in combination with other photoreceptors, regulate photomorphogenetic processes such as seed germination, etiolation, growth inhibition, leaf development, phototropism, shade avoidance, induction of flowering and regulation of the circadian clock [3]. On the other hand, the biological function of the other phytochromes remains mostly unknown. It has been postulated that BphPs act as bilin sensors that can function as

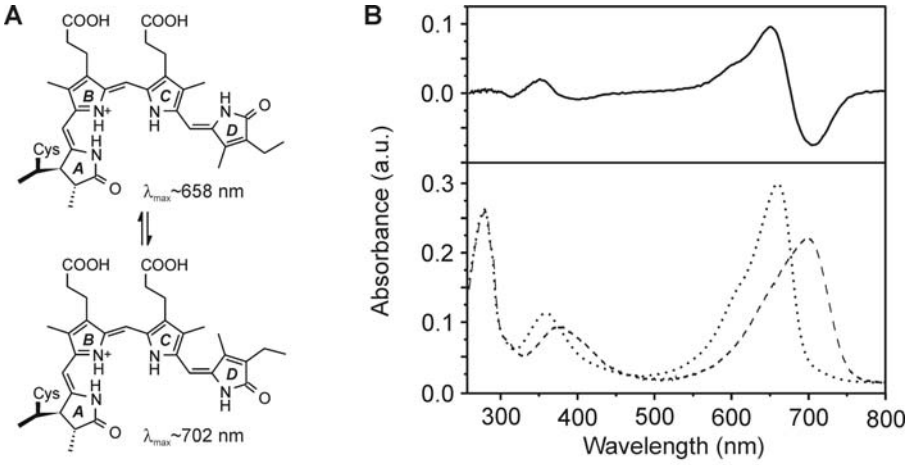

Figure 1.2: Photoconversion of cyanobacterial phytochrome 1 (Cph1). (**A**) Structure of the phycocyanobilin chromophore with *ZZZssa* and *ZZEssa* geometries as assumed in the Pr and Pfr states, respectively. (**B**) Absorption spectrum of Cph1 in the Pr (dotted line), Pfr (dashed line) and Pr-Pfr difference spectrum (full line).

photoreceptors. In particular, it has been proposed that BphPs regulate the biosynthesis of the photosynthetic apparatus in the photosynthetic bacterium *Rhodopseudomonas palustris* [8] and trigger pigment biosynthesis in *Deinococcus radiodurans* and *Rhodospirillum centenum* [9, 10].

1.1.2 The modular domain architecture of phytochromes

All phytochrome families share a common dimeric Y-shaped architecture (Fig. 1.3A) [11–13]. The quaternary structure of each monomer consists of two domains (for review, see [7, 14]). The N-terminal photosensory region binds the bilin cofactor and is composed of three conserved domains, termed P2 or PerARNT-Sim domain, P3 or cGMP phosphodiesterase/adenyl cyclase/FhlA domain, and P4 or PHY domain (uppercase letters are used to denote the Phy domain specifically), while the C-terminal regulatory module contains a histidine kinase or histidine kinase related domain (Fig. 1.3B). Plant Phys have an additional N-terminal extension termed P1 and two additional regulatory PAS domains. Fphs have distinct N-terminal extensions and additional C-terminal response regulator domains. Canonical phytochromes thus consist of a PAS-GAF-PHY N-terminal photosensory module typically combined with

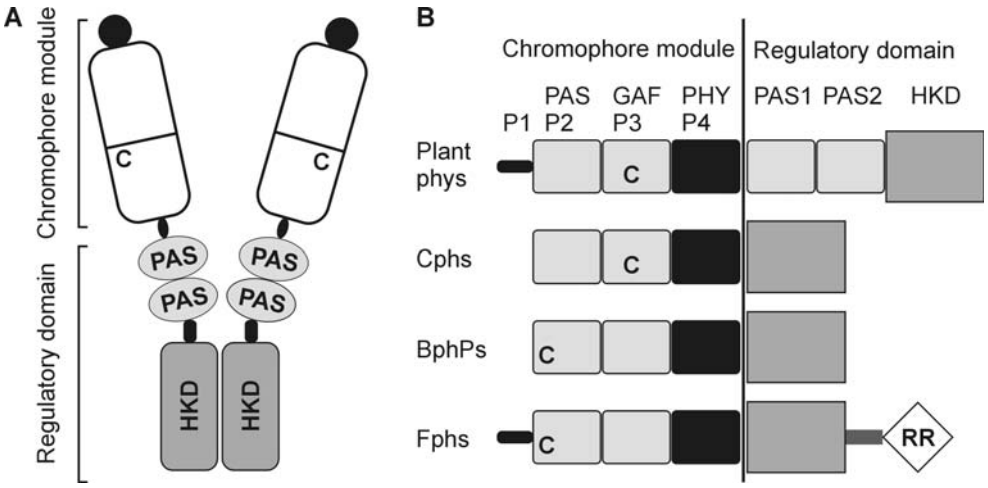

Figure 1.3: Quaternary structure of plant phytochrome in the Pr state adapted from [16] (**A**). Schematic representation of the domain structure of plant Phys, Cphs, BphPs and Fphs phytochromes (**B**). The chromophore location is indicated by **C**.

a C-terminal HKRD module. The concatenation of PAS, GAF, and PHY domains attached to HKRD modules typify all classes of phytochromes and phytochrome-related proteins. For a detailed description of the phytochrome domains, see [15].

1.1.3 The phytochrome chromophore

The bilin or open-chain tetrapyrrole chromophores incorporated in all phytochromes are synthesized from hemes in two steps. First, a heme oxygenase converts the heme into biliverdin (Fig. 1.4), which is directly attached as chromophore of the BphPs and Fphs *via* a thioether linkage at $C3^2$ to a conserved cysteine upstream of the P2/PAS domain [17, 18]. In plants and cyanobacteria, however, BV is further reduced to yield phytochromobilin in higher plants and phycocyanobilin in cyanobacteria and green algae (Fig. 1.4). Both PΦB and PCB bilins are covalently attached at $C3^1$ to a conserved cysteine in the P3/GAF domain of the photosensory core [19–21].

Borucki *et al.* have investigated the autocatalytic assembly of the Cph1 apoprotein with its native PCB chromophore [22]. The first step of the PCB assembly is associated with a major red shift and transfer of oscillator strength from the Soret region to the 680 nm region. This absorption change is due

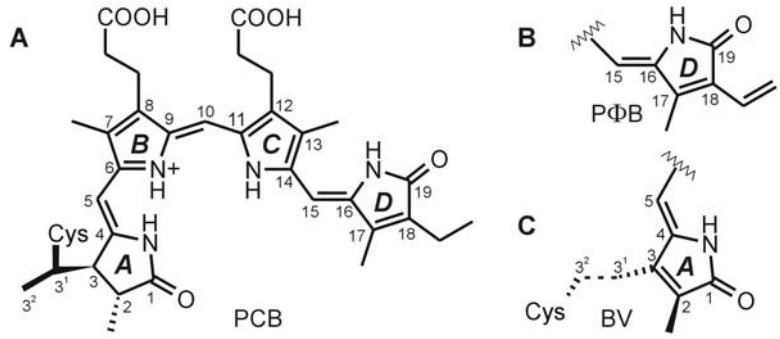

Figure 1.4: Structure of the phycocyanobilin (PCB) in the *ZZZssa* geometry (**A**). Ring ***D*** of phytochromobilin (PΦB, **B**) and ring ***A*** of biliverdin (BV, **C**) are represented. The remainder of these molecules is identic to PCB.

to the formation of the extended conformation of the linear tetrapyrrole, presumably from a *ZZZsss* (5-*Z*, 10-*Z*, 15-*Z*, 5-*syn*, 10-*syn*, 15-*syn*) geometry of the three methine bridges, as present in solution [23, 24], to a *ZZZssa* geometry [25]. Then the protonation of the ring ***B*** nitrogen occurs in the binding pocket. The third step is associated with a blue shift of about 25 nm, which has been attributed to the formation of the covalent bond with a cysteine residue.

The intrinsic photochemical activity of the open-chain tetrapyrrole cofactor inside the chromophore binding domain allows the photoconversion between the Pr ($\lambda_{max} \sim 660$ nm) and Pfr ($\lambda_{max} \sim 710$ nm) states. Using 60 kDa chromopeptides, ^{1}H liquid-state NMR studies revealed that the absorption of red light triggers the *Z*-to-*E* photoisomerization of the C15=C16 double bond [20, 26].

1.1.4 The phytochrome photocycle

The photochemical conversion processes of phytochrome have been intensively investigated. Time-resolved absorption, low temperature and vibrational spectroscopic methods allowed for the identification of three intermediates appearing during the Pr → Pfr pathway (Lumi-R, Meta-R$_a$, and Meta-R$_c$), and at least two intermediates (Lumi-F and Meta-F) during the reverse Pfr → Pr reaction (Fig. 1.5). The first step of the Pr → Pfr conversion is the *Z*-to-*E* photoisomerization of the C15=C16 double bond [20, 26–29]. Ultrafast

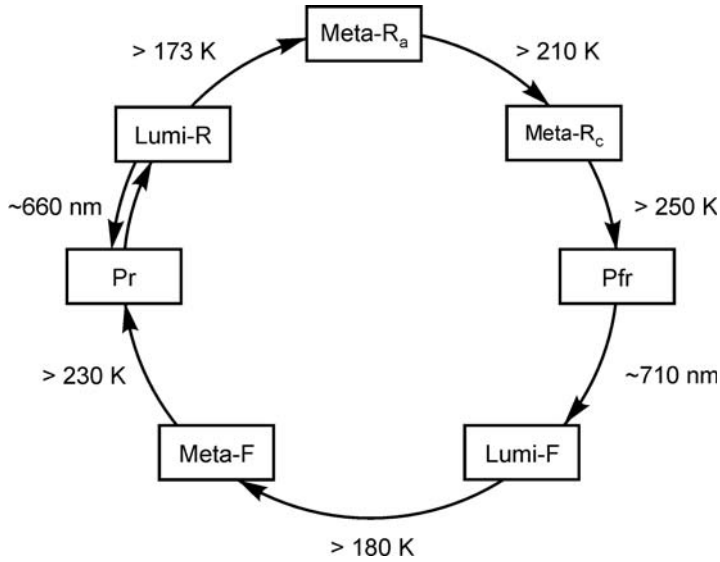

Figure 1.5: Photocycle of the Cph1 phytochrome

Vis/Vis pump-probe spectroscopy and picosecond time-resolved fluorescence spectroscopy at room temperature have determined the time scale of the formation of Lumi-R to be in the picosecond range [30–36]. The extent of the photoreversible Pr → Pfr phototransformation upon red light illumination was determined to be about 0.75 for Cphs [37] and about 0.87 for plant Phys [38]. In both cases, the quantum yield Φ of 0.15 is relatively low. The subsequent reaction steps occur on the microsecond to millisecond time scale. Intermediate states of the photocycle of different Phys have been addressed by Fourier transform infrared and resonance Raman spectroscopy using low-temperature trapping techniques [27, 39–43]. At room temperature, the Meta-R_a state is formed within hundreds of microseconds and decays within milliseconds to the last intermediate before Pfr, called Meta-R_c [27, 39, 42]. The Meta-R_c formation is characterized by a significant red shift of the first absorption maximum and is the key step of the Pfr formation, which occurs within hundreds of milliseconds.

The Pfr → Pr conversion has been investigated less intensively. Until now, two intermediates have been identified, Lumi-F and Meta-F. While the Pr photoreaction occurs in 40-200 ps, the Pfr photoreaction is much faster and occurs on the time scale of a few picoseconds [31,33,35]. Despite intensive

and extensive investigations with vibrational and optical spectroscopy [27,39, 40, 43], the molecular and mechanical characteristics of these intermediates remain to be discovered.

1.1.5 X-ray structures of phytochromes

Until 2005, the study of the structural interactions in phytochrome was limited to indirect methods such as amino acid mutation [44–50]. A breakthrough occurred when the crystallographic studies of the CBDs from *Deinococcus radiodurans* DrBphP [18,51] and *Rhodopseudomonas palustris* RpBphP3 [52] revealed the structures of the PAS and GAF domains and their biliverdin-IXα chromophore in the Pr state. However, these phytochromes lack the PHY domain, which has been shown to be required for Pfr stability [19, 44, 45, 47, 48] and do not undergo full photoconversion between the Pr and Pfr states. The X-ray structure of the complete sensory module (PAS-GAF-PHY tridomain) of the N-terminal part of the cyanobacterial phytochrome 1 (residues 1-514) from *Synechocystis* sp. PCC 6803 in the Pr state has been resolved in 2008 [53]. In the tertiary structure of these three proteins, the PAS domain penetrates the GAF domain to form a knot in which the N-terminal extension passes through the large insert in the GAF domain. The unique feature of the Cph1 structure is a long, tongue-like protrusion from the PHY domain that seals the chromophore pocket (Fig. 1.6A).

Although the comparison between the tertiary structures of these three proteins revealed some differences, most of the chromophore-protein interactions present in the CBD are conserved. The domain architecture and CBD in Cph1Δ2 are presented in Figure 1.6B. The PCB cofactor is covalently attached to the GAF domain by a carbon-thioether link between the $C3^1$ carbon and the sulfur of Cys-259 and adopts a *ZZZssa* geometry at the three methine bridges. The chromophore is twisted by angles of 9.8°, 1.4°, and 26.3° between pyrrole rings ***A*-*B***, ***B*-*C***, and ***C*-*D***, respectively. However, slight rotations around single bonds that are hardly reflected by the crystal structures may cause a more distorted chromophore, a scenario that is supported by a recent investigation utilizing vibrational spectroscopy and density functional theory (DFT) calculations [54]. One of the main features of the chromophore/protein interactions is the occurrence of a very well ordered water molecule (W-3) that participates in a hydrogen-bonding network with the nitrogen atoms of the rings ***A***, ***B***, and ***C***, the His-260 Nδ nitrogen and the

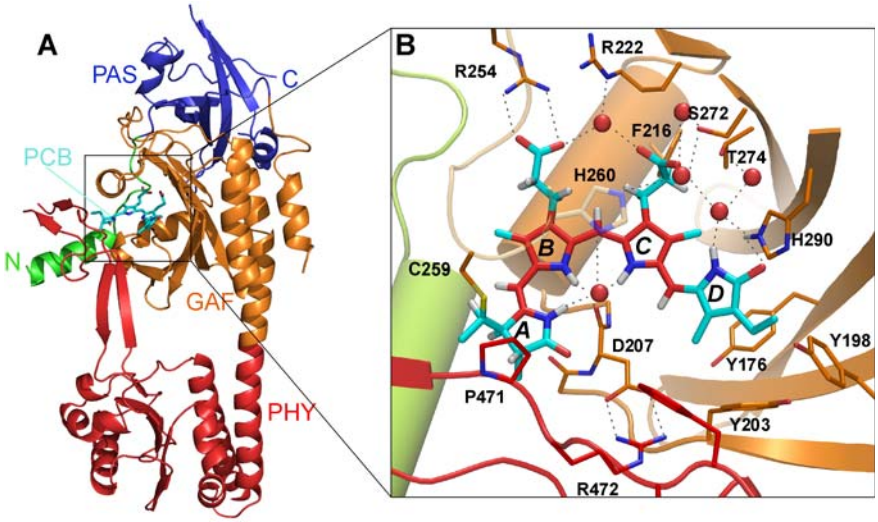

Figure 1.6: Ribbon representation of the sensory module structure of Cph1Δ2 showing the N-terminal α-helix (green) and PAS (blue), GAF (orange) and PHY (red) domains (**A**) and zoom into the chromophore region (**B**).

amide oxygen of Asp-207. The conserved His-290 residue is hydrogen-bonded to the C19 carbonyl of ring ***D*** and is linked to the carboxylic group of the propionic side-chain of ring ***C*** through a water-mediated bridge. In addition, the crystal structure of the CBD shows that the rings ***A***, ***B*** and ***C*** are tightly packed inside the matrix, especially around the C10 atom connecting rings ***B*** and ***C***. In contrast, there is space for ring ***D*** to rotate upon *Z*-to-*E* photoisomerisation of the C15=C16 double bond [53].

The crystal structure of the PaBphP-PCD BphP from *Pseudomonas aeruginosa* with an intact, fully photoactive photosensory core domain in its dark-adapted Pfr state has been determined in 2008 [55]. In this structure, the BV chromophore adopts a *ZZEssa* geometry. Asp-194, Tyr-250, and Ser-459 (equivalent to Asp-207, Tyr-263 and Ser-472 in Cph1Δ2) interact directly with the pyrrole nitrogen of ring ***D***, and Tyr-250, Gln-188, and Ser-459 (Tyr-263, Lys-201 and Ser-472 in Cph1Δ2) are within hydrogen-bonding distance of the C19 carbonyl group of ring ***D***. It is believed that the main features of the PaBphP-PCD BphP structure in its Pfr dark-adapted state are similar to Cphs and plant Phys. However, it has to be kept in mind that the PaBphP-PCD BphP has a low stability in the Pr state and that some residues of the

CBD (Gln-188 or Arg-453) are not conserved along the Phy family.

1.2 Theoretical background of solid-state CP/MAS NMR

1.2.1 Interactions in solid-state NMR

The Zeeman interaction between the nuclear magnetic moment of a spin and the external field **B** is the dominant interaction in NMR. This interaction can be described by the Zeeman Hamiltonian H_z for a magnetic field $\mathbf{B}_0$ along the z-axis

$$H_z = -\gamma^i \hbar I_z B_0, \tag{1.1}$$

where I_z is the z-component of the nuclear spin operator **I**. Although the Zeeman interaction dominates the behavior of the nuclear spin system and determines the quantization z-axis in the theoretical description, it contains little relevant structural information and is removed from the description by a transformation to a frame that is rotating at the NMR frequency along the z-axis [56].

For the spectroscopic applications of NMR, the relevant information originates from the local fields that the nuclear spins "feel". These fields are due to the shielding of the $\mathbf{B}_0$ field by the electron clouds and from the dipolar couplings between spins. For an ensemble of nuclear spins placed in a large magnetic field containing two species, *i.e.*, an abundant I spin system (*e.g.* ^{1}H) with a gyromagnetic ratio γ^I and a resonance frequency ω_{0I} and a dilute S spin system (*e.g.* ^{13}C, ^{15}N) with a gyromagnetic ratio γ^S and a resonance frequency ω_{0S}, the interactions can be described by the chemical shift Hamiltonian H_{CS}, and the homonuclear and heteronuclear dipolar Hamiltonians, H_{D}^{II} and H_{D}^{IS}, respectively. In the rotating frame, this leads to a spin Hamiltonian having the form

$$H = H_{\mathrm{CS}} + H_{\mathrm{D}}^{II} + H_{\mathrm{D}}^{IS}. \tag{1.2}$$

1.2.2 Chemical shielding Hamiltonian

The chemical shielding Hamiltonian expressed as

$$H_{\mathrm{CS}} = -\gamma \mathbf{I} \boldsymbol{\sigma} \mathbf{B_0} \tag{1.3}$$

describes the effect of the electron distribution around the nuclear spin, where $\boldsymbol{\sigma}$ is the chemical shielding tensor.

The electronic distribution around a nucleus in a molecule is rarely spherically symmetric. Since the chemical shielding arises from the electronic surroundings of a nucleus, its value depends on the orientation of the molecule in the magnetic field $\mathbf{B}_0$. This orientation dependence is best described in terms of a chemical shielding tensor, which is a 3×3 matrix that relates the orientation of the magnetic field to the molecular frame in which the induced electronic currents are generated.

The chemical shielding tensor can be placed into its principal axis system, *i.e.*, the reference frame in which it is diagonal and all off-diagonal components are zero, where the principal values of the shielding tensor are σ_{xx}, σ_{yy} and σ_{zz}. In solid-state NMR, the tensor is often represented by

$$\begin{aligned} \sigma_{\text{iso}} &= -\frac{1}{3}(\sigma_{xx} + \sigma_{yy} + \sigma_{zz}), \\ \delta &= \sigma_{zz} - \sigma_{\text{iso}}, \\ \text{and } \eta &= -\frac{\sigma_{xx} - \sigma_{yy}}{\delta}. \end{aligned} \tag{1.4}$$

Here, σ_{iso} is the isotropic value, while δ and η are the anisotropy and asymmetry parameter, respectively [57, 58].

The expression for the anisotropic frequency of a single site in a static sample is given by Equation 1.5 where the orientation dependence of the frequency can be expressed in terms of the polar angles (θ, ϕ) of the $\mathbf{B}_0$ field in the principal axis system [58]:

$$\omega(\theta, \phi) = \delta - \frac{1}{2}(3\cos^2\theta - 1 - \eta - \sin^2\theta\cos 2\phi). \tag{1.5}$$

The chemical shielding Hamiltonian H_{CS} in the principal axis system can be rewritten as

$$H_{\text{CS}} = [\sigma_{\text{iso}}\gamma B_0 + \frac{1}{2}\delta(3\cos^2\theta - 1 - \eta - \sin^2\theta\cos 2\phi)]I_z. \tag{1.6}$$

1.2.3 Dipolar coupling Hamiltonian

The heteronuclear coupling is responsible for much of the broadening observed in the solid-state NMR spectrum. Since each spin represents a nuclear magnetic moment that produces a small magnetic field, every spin "feels" the

magnetic field produced by the nearby spins. The strength of the heteronuclear dipolar coupling is represented by the truncated dipolar Hamiltonian

$$H_{\mathrm{D}}^{IS} = -\frac{\mu_0}{4\pi}\hbar \sum_i \sum_j \frac{\gamma^I \gamma^S}{r_{ij}^3} \frac{1}{2}(3\cos^2\theta_{ij} - 1) 2 I_z^i S_z^j, \tag{1.7}$$

where r_{ij} represents the internuclear distance, μ_0 is the vacuum permeability, γ^I and γ^S are the gyromagnetic ratios of the I and S spins, respectively, and I_z^i and S_z^j are the z-components of the nuclear spin angular momentum operators $\mathbf{I}$ and $\mathbf{S}$, respectively. The angle θ_{ij} describes the orientation of the internuclear vector with respect to the orientation of the external magnetic field. Since the magnitude of the coupling between two nuclear spins has also an r^{-3} distance dependence, the dipolar coupling is a long-range through-space interaction.

Spins also experience a homonuclear dipolar coupling, which results from an interaction between spins of the same species. The homonuclear dipolar Hamiltonian of the I spins is given by

$$H_{\mathrm{D}}^{II} = -\frac{\mu_0}{4\pi}\hbar \sum_i \sum_j \frac{\gamma^I \gamma^S}{r_{ij}^3} \frac{1}{2}(3\cos^2\theta_{ij} - 1)(3 I_z^i S_z^j - \mathbf{I}^i \mathbf{I}^j). \tag{1.8}$$

In this case, r_{ij} represents the internuclear distance and the angle θ_{ij} describes the orientation of the internuclear vector with respect to the orientation of the external magnetic field. Two spins of the same species are able to undergo an energy-conserving "flip-flop" transition in which one spin flips up while the other spin flips down.

1.3 Solid-state NMR techniques

In liquid-state NMR, spectra consist of a series of very sharp signals, which are due to the averaging of the anisotropic NMR interactions by rapid tumbling. By contrast, the full effects of anisotropic or orientation-dependent interactions are observed in solid-state NMR and the resulting signals are generally very broad. In the solid-state, enhancement of peak resolution and signal intensity is obtained under magic angle spinning by the transfer of the ^{1}H magnetization to a dilute spin (^{13}C or ^{15}N) *via* cross-polarization in combination with strong proton decoupling.

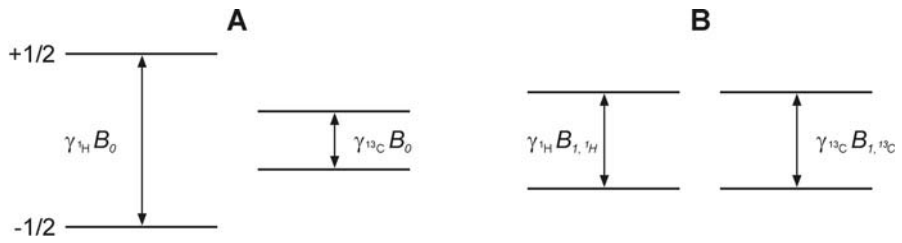

Figure 1.7: Energy levels of the I and S spins. In the laboratory frame, no transfer of magnetization occurs (**A**). In the rotating frame (**B**), the transfer of magnetization is possible due to the application of the RF fields.

1.3.1 Magic angle spinning

As shown in sections 1.2.2 and 1.2.3, the dependence on the molecular interaction is of the form $(3\cos^2\theta - 1)$, where the angle θ describes the orientation of the spin interaction tensors, in particular the chemical shielding and dipolar coupling tensors. In the MAS experiment, the sample is spun rapidly in a cylindrical rotor around a spinning axis oriented at the magic angle ($\theta_{\mathrm{R}} = 54.74°$) with respect to the applied magnetic field $\mathbf{B}_0$ [59–61]. MAS averages the dipolar coupling interactions to zero. In addition, the anisotropic part of the chemical shift disappears under MAS conditions and with fast rotation, the anisotropic line broadening is removed resulting in narrow lines. For a detailed mathematical description of MAS, see [57].

1.3.2 Cross-polarization

Detecting low-γ nuclei such as ^{13}C or ^{15}N is difficult due to their low abundances, low spin polarization and low signal intensity. In addition, dilute spins can exhibit long relaxation times. These drawbacks are overcome by the CP technique, which allows the magnetization to flow from highly polarized nuclei to nuclei with lower polarizations when the two are brought into dipolar contact. In the laboratory frame, the separation between the spin-up and spin-down energy levels do not allow for exchange of magnetization (Fig. 1.7A). Dipolar contact is obtained through the simultaneous application of two external radio-frequency fields satisfying the Hartmann-Hahn condition [62]

$$\alpha_{\mathrm{a}}\gamma^{\mathrm{a}}B_{1\mathrm{a}} = \alpha_{\mathrm{b}}\gamma^{\mathrm{b}}B_{1\mathrm{b}}, \tag{1.9}$$

where γ^{i} and B_{1i} are the gyromagnetic ratio and RF field strength for nucleus i, and $\alpha = [I\ (I + 1)\ -\ m(m\ -\ l)]^{1/2}$ for a transition between the levels m and (m - 1). When both nuclei have $I = 1/2$, this equation reduces to the familiar expression

$$\gamma^{a} B_{1a} = \gamma^{b} B_{1b}. \tag{1.10}$$

One of the RF fields is tuned to the resonance frequency of the I spins and the other to the S spins. As a result, both the magnetization of the I and S spins are rotated around the axis of the applied RF fields. When the nutation frequencies of the I and S spins are equal, an energy-conserving dipolar contact between the two spins is created and the polarization is transferred. The contact is best described in the axes of frames, rotating at both the I and S spin nutation frequencies, in which the spacing between the spin-up and spin-down energy levels is equal for the I and S spins (Fig. 1.7B).

1.3.3 Heteronuclear dipolar decoupling

In solid-state NMR, heteronuclear coupling is responsible for much of the signal broadening. Due to the $(3\cos^2\theta - 1)$ dependence of the heteronuclear interaction, experiments with MAS eliminate the broadening due to the heteronuclear interactions. Another way to obtain signal enhancement is to manipulate the I spins, *e.g.* ^{1}H, in such a way that their interaction with the dilute S spins, *e.g.* ^{13}C or ^{15}N, is averaged to zero. For example, this can be obtained by constantly applying RF power known as continuous wave irradiation, which rotates the I nuclear spins between their spin-up and spin-down states and averages the heteronuclear interactions to zero.

1.3.4 Homonuclear correlation spectroscopy

It has been shown in section 1.3.1 that MAS averages the dipolar coupling and results in signal enhancement. However, MAS also erases the structural information content of these interactions. The ^{13}C-^{1}H dipolar-assisted rotary resonance pulse sequence has been designed by Takegoshi *et al.* [63,64] to reintroduce the ^{13}C-^{1}H dipolar interactions. In this thesis, the DARR sequence has been used to record ^{13}C-^{13}C homonuclear dipolar coupling correlation experiment in the solid state. The DARR sequence (Fig. 1.8A) begins with CP of the ^{1}H magnetization to the nearby ^{13}C nuclei. The ^{13}C-^{1}H dipolar interaction is recovered during t_1 by a continuous wave RF irradiation on ^{1}H

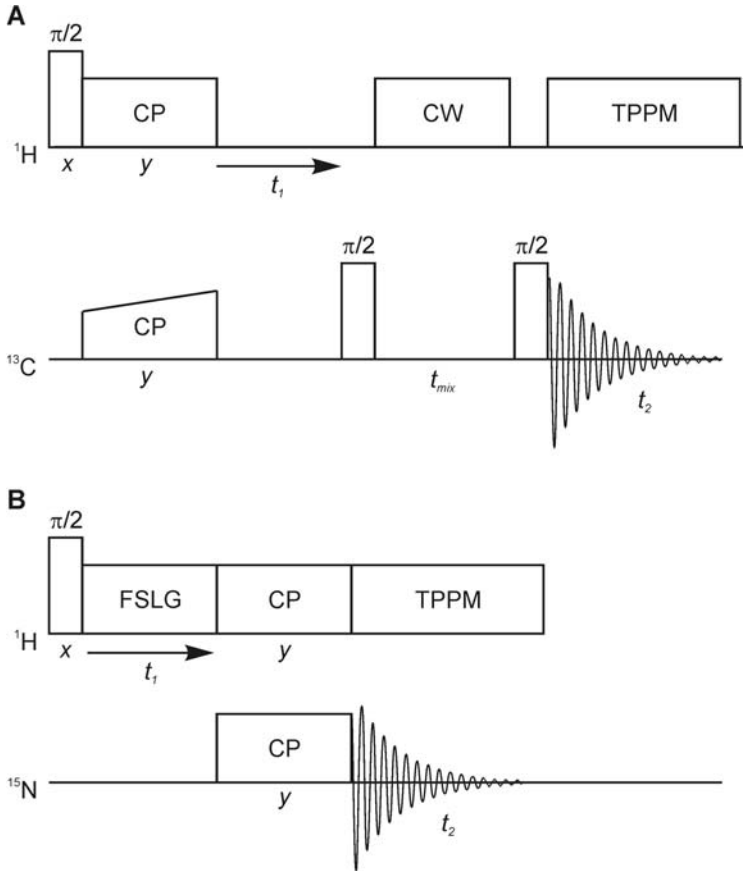

Figure 1.8: Schematic representation of the 2D ^{13}C-^{13}C MAS DARR (**A**) and 2D ^{1}H-^{13}C MAS FSLG (**B**) experiments.

with the intensity ν_1 satisfying the rotary-resonance condition $\nu_1 = n\nu_R$ (n=1 or 2), where ν_R is the rotation frequency. The spectral overlap between two relevant ^{13}C spins is realized between a spinning sideband of one ^{13}C spin and the ^{13}C-^{1}H dipolar pattern of another ^{13}C spin. Then, recoupling due to rotational resonance occurs for the ^{13}C-^{13}C pair and leads to polarization transfer under MAS. Finally, the ^{13}C magnetization is detected in the direct dimension t_2 under two-pulse phase-modulation heteronuclear decoupling [65]. The proton-driven spin diffusion experiment is similar to DARR, the proton decoupling is however switched off during the spin diffusion mixing period.

1.3.5 Heteronuclear correlation spectroscopy

The large homonuclear dipolar couplings of the proton nuclei make their direct detection difficult. In this thesis, a variant of the Lee-Goldburg technique [66], *i.e.* the frequency-switched Lee-Goldburg heteronuclear correlation spectroscopy [67,68] (Fig. 1.8B), is used for the determination of the proton chemical shifts. The ^{1}H magnetization is initially rotated into the xy plane by a $\pi/2$ x-pulse. Directly after the initial pulse, the protons are subject to a train of FSLG pulses for a time t_1. The application of a frequency switched off-resonance RF field between $\omega_{+\Delta LG}$ and $\omega_{-\Delta LG}$ results in an effective field $\mathbf{B}_{\text{eff}}$ in the rotating frame that is inclined at the magic angle with respect to the static magnetic field $\mathbf{B}_0$ [66]. The LG condition is given by Equation 1.11, where ω_1 = -γB$_1$:

$$\pm\Delta\text{LG} = \omega_{\pm\Delta\text{LG}} - \gamma B_0 = \pm\frac{1}{2}\sqrt{2}|\omega_1|. \tag{1.11}$$

The train of FSLG pulses is used to improve the efficiency of the homonuclear proton decoupling. Thus, the magnetization evolves under the ^{1}H chemical shifts and the heteronuclear couplings to ^{13}C nuclei during t_1. After t_1, the ^{1}H magnetization is transferred through CP to the neighboring ^{13}C nuclei for detection in t_2. In this way, the 2D FSLG spectrum correlates broad ^{1}H resonances with the relatively narrow resonances of the ^{13}C nuclei and allows for increased resolution of the proton chemical shifts.

1.4 Aim and scope of this thesis

In this thesis, solid-state MAS NMR spectroscopy has been applied in combination with ^{13}C- and ^{15}N-labeling of the bilin chromophore to study the photochemical machinery of phytochrome.

Chapter 2 deals with the MAS NMR study of free PCB in its microcrystalline state. ^{13}C and ^{15}N labeling of the PCB moiety allows for complete ^{13}C and ^{15}N assignments deduced from 2D ^{13}C-^{13}C and ^{13}C-^{15}N correlation spectroscopy. It is shown that the PCB moieties are present in the crystal in two forms, called A and B, at a ratio A:B = 1:1. In combination with computational methods, a structural model for the PCB dimer is proposed.

Chapter 3 focuses on the electronic ground state of the PCB chromophore in Cph1Δ2 in the parent states Pr and Pfr. The analysis of the isotropic

^{13}C chemical shifts reveals the electronic changes along the conjugated π-system and the modification of chromophore/protein interactions. The NMR data shown in this chapter are used to present a model for signal transduction in phytochrome.

Chapter 4 describes the Pfr $\rightarrow$ Pr back-reaction. The two intermediates, Lumi-F and Meta-F, have been thermally trapped inside the magnet at low temperature and studied by ^{1}H, ^{13}C and ^{15}N MAS NMR spectroscopy. The results show that the back-reaction proceeds in two steps and provide further insight into the mechanism of signal transduction in phytochrome.

Chapter 5 provides a general discussion on the results and conclusions obtained in this thesis. Finally, an outlook to future experiments is presented.